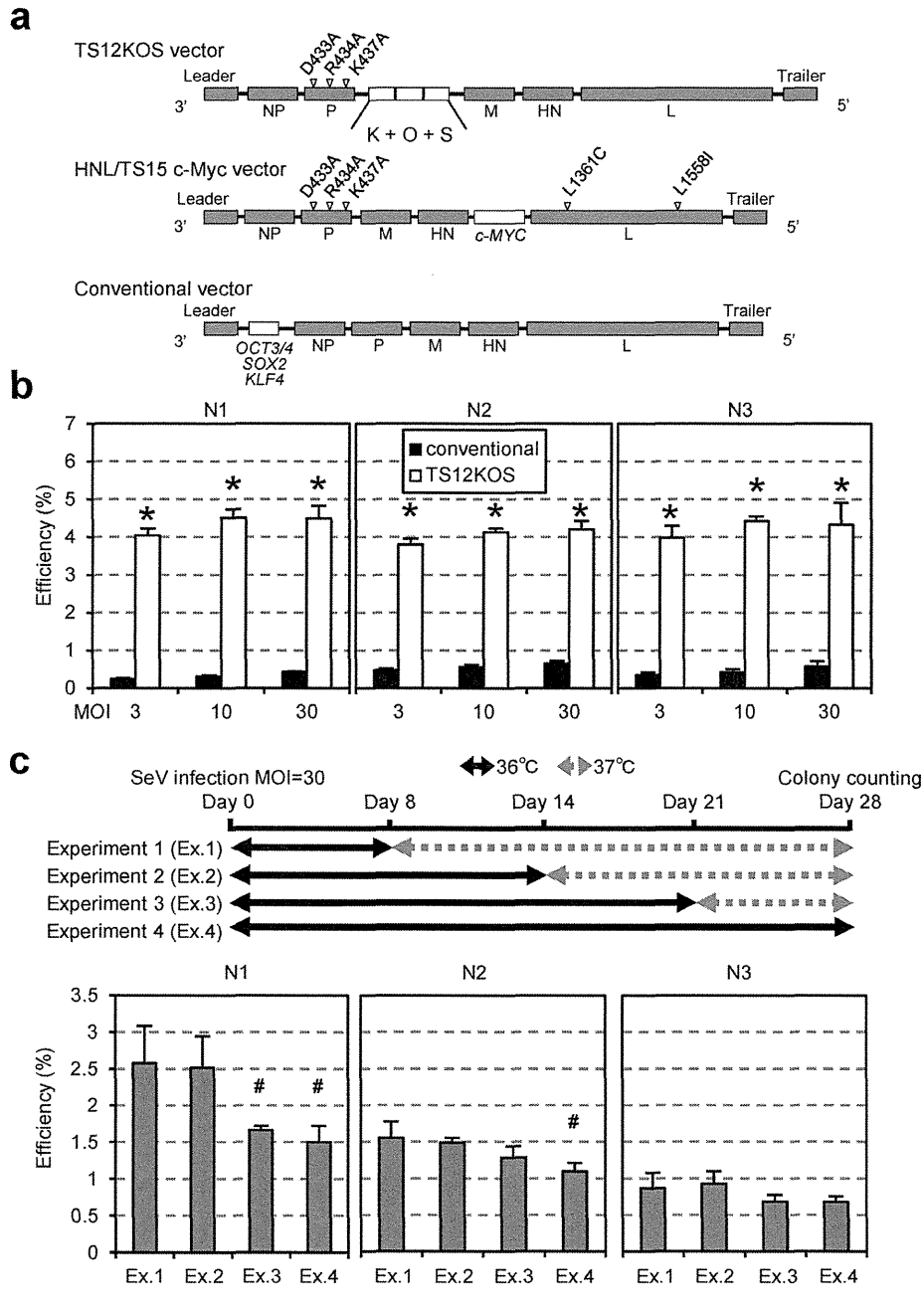
a
TS12KOS vector
Leader
D433A
R434A
K437A
Trailer
3'
NP
P
K + O + S
M
HN
L
5'
HNL/TS15 c-Myc vector
L1361C
L1558I
c-MYC
Conventional vector
OCT3/4
SOX2
KLF4
b
N1
N2
N3
conventional
TS12KOS
Efficiency (%)
MOI 3
10
30
c
SeV infection MOI=30
Day 0
Day 8
Day 14
Day 21
Colony counting
Day 28
36°C
37°C
Experiment 1 (Ex.1)
Experiment 2 (Ex.2)
Experiment 3 (Ex.3)
Experiment 4 (Ex.4)
Ex.1
Ex.2
Ex.3
Ex.4
d
Time of temperature shift
Passage 1
Passage 2
Conventional vector
0/22 (0 %)
0/22 (0 %)
TS12KOS vector
19/23 (84.7 %)
15/23 (65.2 %)

**Figure 1. Generation of a new temperature-sensitive Sendai virus vector, TS12KOS.** (**a**) Comparison of schematic structures among the newly constructed Sendai virus (SeV) vector, TS12KOS, and previous vectors. The TS12KOS vector contains three point mutations in the RNA polymerase–related gene (P) and carries the coding sequences of *KLF4* (K), *OCT3/4* (O), and *SOX2* (S) in the KOS direction. In comparison, the HNL/TS15 c-Myc vector carries two additional mutations, L1361C and L1558I, in the large polymerase (L) gene and an exogenous c-*MYC* cDNA sequence inserted between the hemagglutinin-neuraminidase (HN) and L genes, and the conventional vectors individually carry three reprogramming factors as indicated. (**b**) iPS cell generation from human skin-derived fibroblasts. The efficiency of iPS cell generation was significantly higher using the TS12KOS vector than with the conventional vectors at all multiplicities of infection (MOI) tested. iPSC colonies were identified on day 28 of induction by the appearance of alkaline phosphatase-positive ($AP^+$) colonies with embryonic stem (ES) cell-like colony morphology. N1, N2, and N3 represent individual healthy volunteers. Experiments were conducted in triplicate (mean ± SD). $^*P<0.01$, TS12KOS vector versus conventional vectors, Student's t-test. (**c**) Temperature shift from 37°C to 36°C for the indicated periods in iPSC generation. Data are means ± SD of three independent experiments. $^{\#}P<0.05$, Experiment 2, 3 and 4 versus Experiment 1. Student's t-test. (**d**) Nested RT-PCR analysis of SeV vector elimination after the temperature shift from 37°C to 38°C in human fibroblast-derived iPSCs. The elimination of TS12KOS vector was faster than the conventional vectors.

doi:10.1371/journal.pone.0113052.g001

Based on previous findings that L-*MYC* is safer than c-*MYC* due to a lower incidence of tumorigenicity, we next examined the effect of replacing the c-*MYC* cDNA sequences with L-*MYC* cDNA sequences in the HNL/TS15 c-MYC SeV vector (Fig. S1a) [25]. The frequency of colonies with ALP+ and ESC-like morphology was lower using the L-*MYC* vector than with the original HNL/TS15 c-MYC vector (Fig. S1b), despite the L-*MYC* gene showing higher expression levels (data not shown).

Because Glis1 can enhance iPSC generation, we also constructed and tested various SeV vectors carrying *GLIS1* sequences (Fig. S1a, c) [26]. Unexpectedly, Glis1 expression did not augment the colony formation from human skin-derived fibroblasts with or without c-Myc, suggesting that Glis1 does not play a part in iPSC induction with SeV vector (Fig. S1c).

## Characterization of human iPS cells generated with new virus vector

Our ultimate goal is to develop safe and efficient vectors to generate iPSCs from both human and primate peripheral blood cells. When we stimulated human peripheral T lymphocytes with both anti-CD3 antibody and interleukin 2, and then infected them with SeV vectors, iPSC generation was significantly more efficient using the TS12KOS vector than with the conventional SeV vectors (Fig. 2a). In conventional SeV infections, temperature shifts from 37℃ to 38℃ at passages 1 and 2 induced no elimination of virus from the iPSC clones (Fig. 2b). In contrast, when TS12KOS vector was used under the same conditions, 65% and 47%, respectively, of the clones were negative for viral genome (Fig. 2b). Therefore, similar to the results obtained with fibroblasts, the elimination of TS12KOS vector from iPS-like cells derived from peripheral T lymphocytes was faster than that observed for the conventional SeV vectors.

The iPSC lines derived from skin fibroblasts and peripheral T lymphocytes induced by TS12KOS vector exhibited a typically ESC-like morphology and expressed a set of typical markers for pluripotency (Fig. 2c, d). These iPSC lines

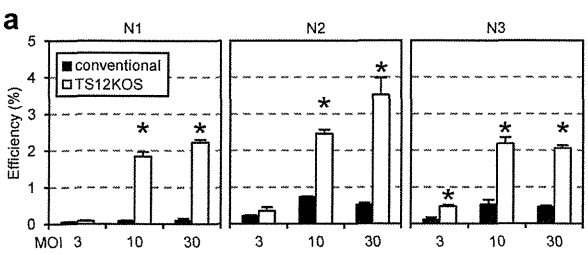


b

| | Time of temperature shift | |
|---|---|---|
| | Passage 1 | Passage 2 |
| Conventional vector | 0/18 (0 %) | 0/18 (0 %) |
| TS12KOS vector | 15/23 (65.2 %) | 11/23 (47.8 %) |

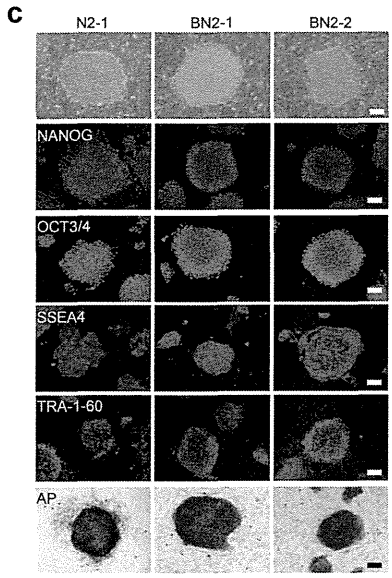


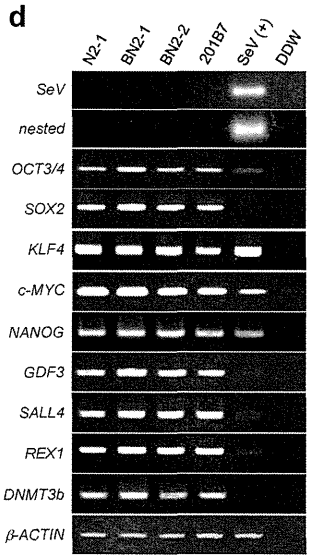


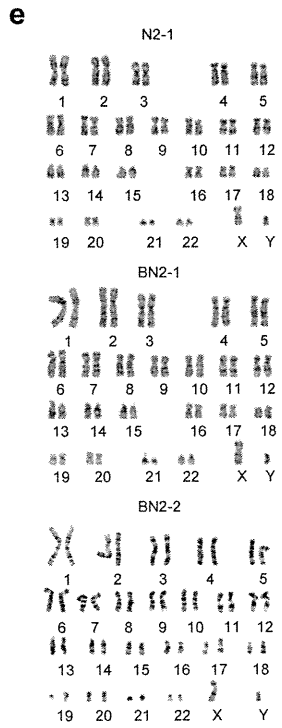


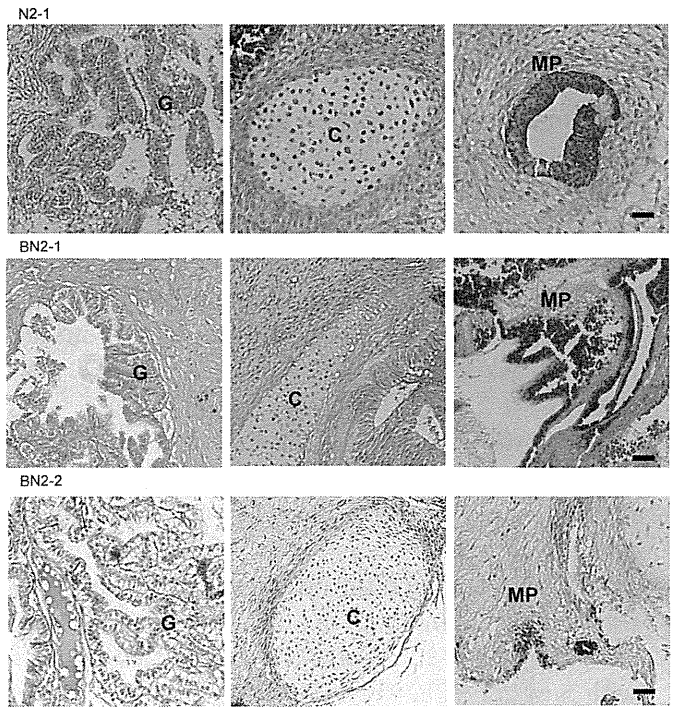

**Figure 2. Characterization of human iPSCs generated by the TS12KOS vector.** (a) iPSC generation from human peripheral blood cells. Experiments were conducted in triplicate (mean ± SD). N1, N2, and N3 indicate individual healthy volunteers. *$P<0.01$, TS12KOS vector versus conventional vectors, Student's t-test. (b) Nested RT-PCR analysis of the elimination of SeV vectors after the temperature shift from 37°C to 38°C. (c) Phase contrast images, immunofluorescence for pluripotency markers, and alkaline phosphatase (AP) staining of iPSC lines. The iPSC lines N2-1 and BN2-1 and BN2-2 were derived from the skin-derived fibroblasts and blood cells of N2 healthy volunteer, respectively. Scale bars, 200 μm. (d) RT-PCR analysis of Sendai virus and human ES cell markers. SeV, first RT-PCR for SeV; nested, nested RT-PCR for SeV; 201B7, control human iPSC line; SeV(+), Day 7 SeV-infected human fibroblasts. (e) Chromosomal analyses of iPSC lines generated with the TS12KOS vector. (f) Tissue morphology of a representative teratoma derived from iPSC lines generated with the TS12KOS vector. G, glandular structure (endoderm); C, cartilage (mesoderm); MP, melanin pigment (ectoderm). Scale bars, 100 μm.

doi:10.1371/journal.pone.0113052.g002

had a normal 46 XY karyotype even after the temperature upshift and culturing for more than 10 passages (Fig. 2e). To confirm the pluripotency of the clonal lines, we transplanted the lines into the testis of immunodeficient mice. Twelve weeks after injection, the iPSC lines tested formed teratomas that contained derivatives of all three germ layers (Fig. 2f). Based on these findings, we conclude that the iPSC lines generated with TS12KOS vector meet the criteria of iPSCs.

## Establishment of chimpanzee iPS cells

Next we used the TS12KOS vector to establish iPSC lines from the blood cells of two chimpanzee individuals, with the ultimate goal of overcoming the limited availability of chimpanzee skin-fibroblasts for human medical use. Using the same protocol as for human blood cells, we could establish chimpanzee blood cell-derived iPSCs (Fig. 3a). However, the frequency was relatively low and only one cell line that carries the normal karyotype could be established (Experiment 1 in Fig. 3a). To optimize the induction conditions, we conducted *in vitro* human T lymphocyte stimulations with anti-CD3, Phytohaemagglutinin (PHA), or Concanavalin A (Con A), and similarly generated iPSCs from human peripheral mononuclear cells (PMNCs) using all three agents, with PHA stimulation the most efficient (Fig. 3b). The morphology of iPSC colonies derived from the anti-CD3- and PHA-stimulated PMNCs was distinct from colonies derived from the Con A-stimulated PMNCs (Fig 3c), which produced flat colonies with clearer and sharper edges than those derived from CD3- and PHA-stimulated PMNCs. In addition, many of the iPSC colonies derived from CD3- and PHA-stimulated PMNCs contained $AP^+$ cells in the center only (Fig. 3c). Together, these results suggested that colonies derived from Con A-stimulated PMNCs most closely fulfill the accepted criteria of iPSCs. Therefore, Con A was used in the following experiment 2 and 3 (Fig. 3a).

In addition, we changed the virus titer for infection from MOI 10 to 30 and the fibroblast growth factor 2 (FGF2) concentration from 5 ng/ml to 30 ng/ml during the iPSC induction (Fig. S2). The FGF2 change was based on a study of common marmosets, another nonhuman primate, which used 20 ng/ml FGF2 and treated the cultures with sodium butyrate (NaB) during reprogramming to enhance the iPSC colony number [7, 27]. In human blood cells, the efficiency of iPSC generation with 30 ng/ml FGF2 is slightly but not significantly lower than that with 5 ng/ml FGF2 (Fig. S3). Interestingly, these modifications improved the

**a**

| | Chimpanzee | | | Stimulation Factor | SeV | MOI | FGF2 (ng/ml) | Frequency average(%) | Picked up Colonies | SeV(-) Colonies | Efficiency average(%) | Karyotype Normal No/Total No | Clone Name |
|---|---|---|---|---|---|---|---|---|---|---|---|---|---|
| | No | Age | Sex | | | | | | | | | | |
| Experiment 1 | 1 | 36 | Female | anti-CD3 Ab | New | 10 | 5 | 0.0016 | 2 | 2 | 100 | 1/2 | C101 |
| Experiment 2 | 2 | 46 | Female | ConA | New | 30 | 30 | 0.32 | 29 | 17 | 58.62 | 2/3 | C201 C205 |
| Experiment 3 | | | | ConA | Conv | 30 | 30 | 0.073 | 11 | 2 | 18.18 | 1/2 | C402 |

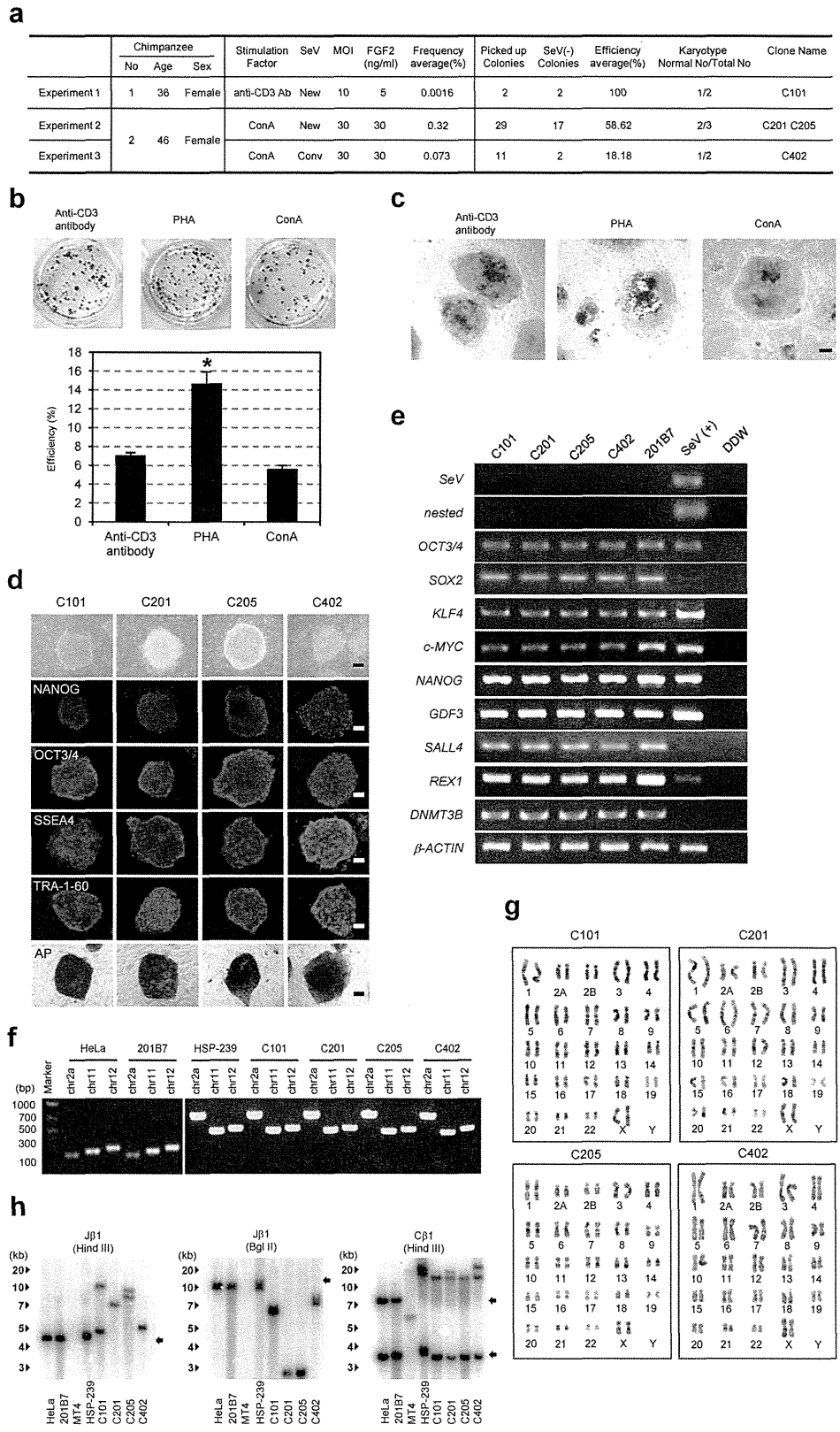

**Figure 3. Generation of chimpanzee iPSCs with the TS12KOS vector.** (**a**) Summary of chimpanzee iPSC generation. iPSCs were generated from the blood cells of two chimpanzee individuals with TS12KOS or the conventional SeV vectors. (**b**) Effect of the T lymphocyte stimulation on iPSC generation. Experiments were conducted in triplicate (mean ± SD). *$P<0.01$, PHA versus anti-CD3 antibody or Con A stimulations, Student's t-test. (**c**) Colony morphology and AP staining of iPSCs from stimulated T lymphocytes. (**d**) Phase contrast images, immunofluorescence for pluripotency markers, and alkaline phosphatase (AP) staining of chimpanzee iPSC lines. C101, C201, C205, and C402 are described in **Fig. 3a**. Scale bars, 200 μm. (**e**) RT-PCR analysis of SeV and human ES cell markers. SeV, first RT-PCR for SeV; nested, nested RT-PCR for SeV; 201B7, control human iPSC line; SeV(+), Day 7 SeV-infected human fibroblasts. (**f**) PCR products with primers that can distinguish chimpanzee and human genomes. Chimpanzee PCR products; 782, 472 and 504 bps, Human PCR products; 203, 245, 278 bps. (**g**) Chromosomal analyses of chimpanzee iPSC lines generated with the TS12KOS vector. (**h**) TCR gene recombination. Genes from the chimpanzee iPSC lines were digested with the indicated enzymes and hybridized with the TCR probes by Southern blotting. Arrows indicate the germ bands of TCR genes. HeLa and 201B7: human cell lines, MT4: human T cell line, HSP-239: chimpanzee T cell line.

doi:10.1371/journal.pone.0113052.g003

colony frequency and provided many more iPSC colonies during the second round of iPSC induction (Experiment 2 in Fig. 3a). However, the efficiency of iPSC generation from chimpanzee PMNCs was still lower than that from human blood cells (0.32% vs. 2%, Fig. 3a). We tried picking up the colonies again and expanded them, before shifting the culturing temperature to 38℃ for three days at passage 1 to eliminate the Sendai virus (Fig. 3a). The rate of virus elimination from the chimpanzee iPSCs was similar to that from human iPSCs (65.2% vs. 58.6%).

We then compared the efficiency of iPSC generation with TS12KOS vector to that with the conventional SeV vectors (Experiment 3 in Fig. 3a). Although a high titer (MOI 30) of the conventional SeV vectors could generate chimpanzee iPSCs, TS12KOS vector showed a higher efficiency of iPSC generation (0.073% for the conventional vectors vs. 0.32%, Fig. 3a). Similarly, the elimination rate of SeV was lower than that observed with the conventional vectors, suggesting that our new vector could more efficiently generate the transgene-free iPSCs from chimpanzee blood cells than the conventional SeV vectors.

The chimpanzee iPSC lines exhibited ESC-like morphology and expressed a set of pluripotent markers (Fig. 3d, e), with nested RT-PCR analysis determining that the iPSC lines were negative for SeV genomic material (Fig. 3e). To confirm that these cells were truly derived from chimpanzee, we also performed genomic PCR using chimpanzee-specific primers (Fig. 3f), with different PCR product sizes allowing us to easily distinguish between chimpanzee and human genes and confirming that the chimpanzee-derived samples contained no human DNA fragments [28]. Karyotype analyses showed that the iPSC lines had a normal karyotype, 48XX, further confirming that the iPSC lines were derived from chimpanzee (Fig. 3g).

To investigate the cellular origin of the chimpanzee iPSCs, we performed Southern blot analyses with probes specific for T cell receptor (TCR) DNA ( Fig. 3h) [29]. Rearranged bands were detected in all iPSC lines, indicating that they were derived from the chimpanzee T lymphocytes.

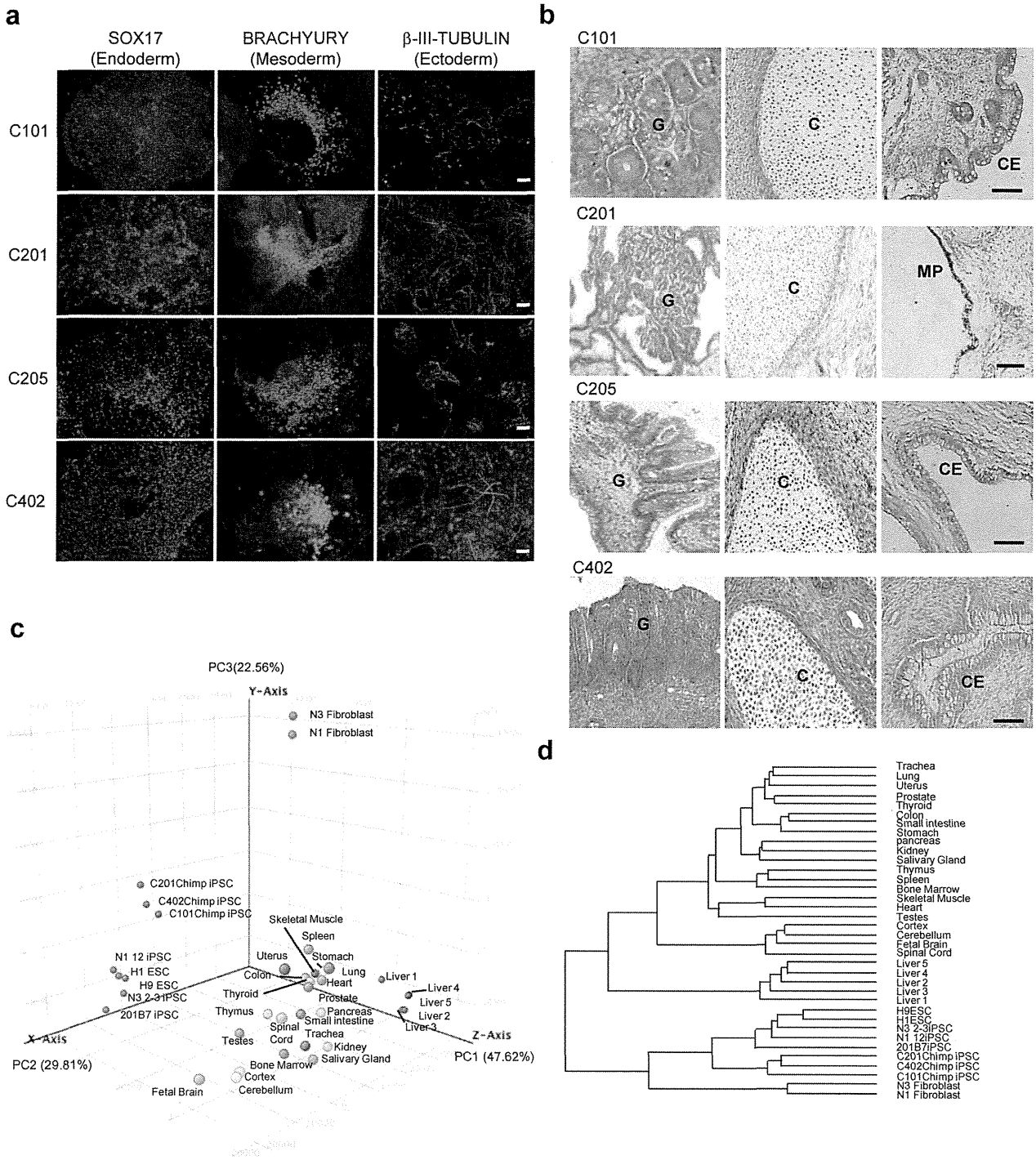


**Figure 4. Characterization of chimpanzee iPSCs.** (**a**) Differentiation into three germ layers in vitro. The chimpanzee iPSC lines can generate SOX17$^+$ (endoderm), BRACHYURY$^+$ (mesoderm), and βIII-tubulin$^+$ (ectoderm) cells. Scale bars, 100 μm. (**b**) Tissue morphology of a representative teratoma derived from the chimpanzee iPSC lines generated with TS12KOS vector. G, glandular structure (endoderm); C, cartilage (mesoderm); CE, Cuboidal Epithelium structure (ectoderm); MP, melanin pigment (ectoderm). Scale bars, 100 μm. (**c**) Principal Component Analysis. All data sets were classified into three principal components, PC1 (47.62%), PC2 (29.81%), and PC3 (22.56%), and then simplified into three-dimensional scores. Percentage shows the portion of variance in each component. The position of chimpanzee iPSC lines is closely placed to that of human ESCs and iPSCs. (**d**) Hierarchical

clustering of chimpanzee iPSCs, human iPSCs and ESCs. The data sets of all genes investigated were clustered according to Euclidean distance metrics. The data sets of chimpanzee iPSCs, human ESC and iPSC lines, and various human tissues were classified into separate branches. The datasets of human ESCs and various tissues referred for Gene Expression Omnibus datasets, GSE22167 and GSE33846, respectively.

doi:10.1371/journal.pone.0113052.g004

### Characterization of chimpanzee iPSC lines

Finally, we investigated the differentiation potential of the chimpanzee iPSCs lines by evaluating in vitro differentiation and teratoma formation (Fig. 4a, b). The appropriate culture conditions induced differentiation into cells representing all three germ layers, ectoderm (βIII-tubulin-positive), mesoderm (BRACHYURY-positive), and endoderm (SOX17-positive) (Fig. 4a). Consistent with this finding, histological analysis revealed that formed teratomas contained descendant markers of all three germ cell layers such as cuboidal epithelia, melanin pigment, cartilage, muscle, and various glandular structures (Fig. 4b). Taken together, the chimpanzee-derived iPSC lines fulfilled the criteria for iPSCs.

We used microarray analysis to further characterize the chimpanzee iPSC lines. The patterns of global gene expression of three chimpanzee iPSC lines were similar to those of human iPSC lines (Fig. 4c). Principal component analysis (PCA) and hierarchical clustering of all genes was conducted to determine overall differences in transcription levels between chimpanzee- and human-derived iPSC lines. Data from human ESCs, iPSCs, fibroblasts, and various tissues were analyzed together with those from chimpanzee iPSCs. Although the chimpanzee iPSC lines were derived from different individuals, their data were grouped by PCA and placed close to those of human ESCs and iPSCs (Fig. 4c). The gene-expression profiles of chimpanzee iPSCs were grouped closely to human ESCs and iPSCs in the same branch, and distinctly separated from the branch containing gene profiles of various human tissues (Fig. 4d). These results suggested that the global gene expression patterns of chimpanzee iPSC lines are generally similar to those of human ESCs and iPSCs.

## Discussion

We developed a new temperature-sensitive SeV vector, TS12KOS, and herein demonstrated it to be an efficient tool for generating iPSCs from both human skin fibroblasts and peripheral blood cells. Using this vector, we also generated chimpanzee iPSC lines from peripheral blood cells.

The iPSCs established with our TS12KOS vector could be made virus-free simply by shifting the temperature from 37℃ to 38℃ for 3 days, and transgene-free iPSCs could be generated within a week of isolating the iPSC colonies. Unlike previous techniques that don't use SeV vectors, this system does not require multiple cycles of infection. Furthermore, the efficiency of iPSC generation achieved was 20~100 times higher than that obtained using techniques such as retrovirus, lentivirus, or plasmid vectors [5, 15, 21].

Consideration of the cell source is important when applying iPSC technology to clinical medicine. Although skin fibroblasts are the most common cell type used for generating iPSCs, we consider that peripheral blood cells are preferable because collection is less invasive and is suitable for children and patients with skin or coagulopathy disorders. Here, we demonstrated that the TS12KOS vector generates iPSCs from both skin fibroblasts (~4%) and peripheral blood cells (~2%) with high efficiency.

Overexpression of the four 'reprogramming' factors needed to generate iPSCs was initially mediated by lentivirus and retrovirus vectors in human skin-derived fibroblasts [5, 15]. Although these gene expression systems are stable, they have two potential problems in that the genes encoding the four factors are integrated into the host genome and remain in the resultant iPSCs, and there is a risk of insertional mutagenesis, which can facilitate tumorigenesis *in vivo* [30]. The development of efficient and safe reprograming methods based on using Cre/loxP recombination systems, adenovirus vector, piggyback transposons, microRNA, and protein has suffered from a low frequency of iPSC colony generation, a need for repetitive induction, and retention of a short length of foreign DNA in the host genome [16–18, 31, 32]. A recent study showed that episomal plasmid vectors, which rarely integrate into the host genome, can be used to generate iPSCs from blood cells; however, the efficiency was low (~0.1%) and factors such as p53 knock-down and the transient expression of Epstein-Barr virus nuclear antigen (EBNA) were required in addition to the four reprogramming factors [21]. To overcome these remaining iPSC issues, in this study we developed a new type of SeV vector that can easily and efficiently provide transgene-free iPSC lines from human and chimpanzee blood cells. SeV vectors are minus-strand RNA viruses that express a gene of interest without integration into the host genome [33]. Thus, our vector can overcome the obstacles described above.

The iPSCs derived from nonhuman primates are useful tools for regenerative medicine research because of the similarities in anatomy and physiology between those mammalian species and human, and chimpanzee is a particularly useful such model [9, 10]. Chimpanzee and human share much of their genomic DNA sequences, with only ~1.2% difference [34]. To this end, we also generated transgene-free iPSC lines from chimpanzee blood cells using the new SeV vector. The efficiency of iPSC generation from chimpanzee blood was lower than that from human blood. Stimulation methods of T lymphocytes and human-derived reprogramming factors may affect the efficiency. Nevertheless, further studies are necessary to improve the efficiency of iPSC generation from chimpanzee blood. Recently, other group established the chimpanzee iPSC lines from skin-derived fibroblasts with the retrovirus vector [35]. However, it is difficult in collecting many chimpanzee-derived fibroblasts because of breeding limitation for medical use. Our new vector can easily provide the transgene-free iPSCs from the chimpanzee blood cells that is less limited than other tissues.

The chimpanzee iPSC lines established here showed the requisite pluripotency and other features of established iPSCs and thus could provide us with alternative and highly valuable tools. First, they could be used to generate fresh chimpanzee

cells, which are valuable cell models and difficult to derive from the animal itself due to breeding limitations. For example, neural cells derived from chimpanzee iPSCs could permit us to study neural development and function, and thus facilitate discovery and increased understanding of the substantial neurological differences between human and chimpanzee despite the largely identical genomes.

Furthermore, the technology used herein could be applied to generate iPSCs from nonhuman primates other than chimpanzees. SeV can infect the blood cells of rhesus monkeys, Macaca fascicularis and marmosets, suggesting that our new vector could also easily induce cell reprogramming and iPSC generation from their blood cells [36, 37]. These approaches are expected to improve our ability to better understand and interrogate the distinguishing traits of human and potentially open up a new field in studying the development of human capacity during evolution.

## Methods

### iPSC Generation and maintenance

All experimental procedures of human samples were approved by the ethics committees, " Ethics committee for Epidemiological and General Research at the Faculty of Life Science, Kumamoto University", "Ethics committee for Human genome and Gene analysis Research at the Faculty of Life Sciences, Kumamoto University" and "Ethics committee for clinical research and advanced medical technology, Kumamoto University" (approval numbers 318, 153 and 1018, respectively) and conformed to the human sample use guidelines of the ethics committees. After explaining our study, the volunteers agreed with our study and signed the sheets of written informed consent.

Human skin biopsies and peripheral blood were collected from healthy volunteers following informed consent under protocols approved by the ethics committee assigning authors. For human fibroblast generation, skin samples were minced and cultured in Dulbecco's modified essential medium (DMEM, Life Technologies) supplemented with 10% fetal bovine serum (FBS). The subsequent fibroblast cultures were expanded for iPS cell induction.

The use of the chimpanzees during the experimental period adhered to the Guidelines for Care and Use of Nonhuman Primates (2010) of the Primate Research Institute of Kyoto University. The ethical committee of the Primate Research Institute of Kyoto University approved the protocols of experimental procedures in this study (Permit Number: 2012-134). Blood samples were obtained from two individuals, Puchi (GAIN-ID:0436) and Ai (GAIN-ID:0434), for routine veterinary and microbiological examination under ketamine anesthesia, and all efforts were made to minimize suffering.

To generate iPS cells from peripheral blood cells, mononuclear cells (MNCs) were isolated by Ficoll gradient method. To stimulate T lymphocytes, MNCs were cultured on anti-CD3 antibody-coated dishes in KBM502 medium (KOHJIN BIO) or RPMI-1640 medium (Invitrogen) supplemented with 10% FBS and IL-2

for five days. In some experiments, instead of anti-CD3 antibody (eBioScience), 10 μg/ml Phytohemagglutinin (PHA, SIGMA) or 1 μg/ml Concanavalin A (Con A, SIGMA) were used for the stimulation.

iPSCs were generated from human skin-derived fibroblasts and human- and chimpanzee-stimulated T lymphocytes as described previously [20]. Briefly, $1 \times 10^5$ of the MNCs per well of 48-well plate and $5 \times 10^5$ cells of the fibroblasts per well of 6-well plate were seeded one day before infection and then were infected with Sendai virus (SeV) vectors at various multiplicity of infection (MOI) including three, ten and thirty. After two-day culturing for blood cells and seven-day culturing for fibroblasts, the cells infected were harvested by trypsin and re-plated at $5 \times 10^4$ cells per 60 mm dish on the mitomycin C (MMC)-treated mouse embryonic fibroblast (MEF) feeder cells. Next day, the medium was replaced in human iPS cell medium. The cultures with new Sendai virus infection were incubated at 36℃ for one week. From 18 to 25 days after infection, colonies were picked up and re-cultured again in the iPS cell medium. In some experiments, FGF2 concentration was modified from 5 ng/ml to 30 ng/ml and NaB was added on day 2 in the iPSC induction. To remove Sendai virus, the temperature of culture shifts from 37℃ to 38℃ for three days at passage 1 or 2 of iPSCs.

Human and chimpanzee iPSC lines were maintained on MMC-treated MEF feeder cells in the iPS medium containing DMEM/F12 (SIGMA) supplemented with 20% KNOCKOUT serum replacement (KSR, Invitrogen), 2 mM L-glutamine (Life technologies), 0.1 mM nonessential amino acids (NEAA, SIGMA), 0.1 mM 2-mercaptoethanol (2ME, SIGMA), 0.5% penicillin and streptomycin (Nacalai Tesque, Japan) and 5 ng/ml or 30 ng/ml basic fibroblast growth factor (bFGF, WAKO, Japan).

## Chimpanzee rearing

At the Primate Research Institute of Kyoto University, the subject chimpanzees lived in two mixed-sex groups in an outdoor enclosure that connected to several inside rooms. The outdoor enclosure was separated into two compartments: one was a 700-$m^2$ outdoor compound with 15-m-high climbing frames, a small stream and numerous trees; the other was a 250-$m^2$ outdoor compound with climbing frames and two small streams. Chimpanzees could freely access the outdoor enclosure and inside room at all times. The chimpanzees were fed seasonal fruits and vegetables, along with monkey pellets three times per day and were provided feeding-enrichment items between meals on a few occasions.

## Generation of Sendai virus (SeV) vectors

Generation and production of temperature-sensitive Sendai virus vectors were performed as described previously [22]. The conventional type of SeV vectors carrying Oct3/4, Sox2, Klf4 and c-Myc were also generated as described previously [22]. To generate TS12 vector, three mutations including D433A, R434A and K437A were introduced into the polymerase-related gene *P*. For TS15 vector

generation, three other mutations, Y942H, L1361C, and L1558I, were inserted into polymerase-related genes *L* of TS12. For "three-in-one" vector, human *KLF4*, *OCT3/4* and *SOX2* genes were inserted between *P* and *M* gene-encoding region in order as described in Fig. 1A. Each gene was sandwiched by *E* (End), *I* (Intervening) and *S* (Start) sequences.

## Karyotype analysis

G band analyses of chromosome were performed by Nihon Gene Research Laboratories. Inc. (Sendai, Japan), according to the manufacturer's protocol.

## DNA and RNA Isolations and PCR

Genomic DNA was extracted from chimpanzee iPSC lines as described previously [38]. Total RNA was purified with Sepasol Super G reagent (Nacalai Tesque, Japan). Total RNA was transcribed to DNA with Superscript III (Invitrogen) and randam primers (Invitrogen). Genomic PCR and RT-PCR was performed with QuickTaq (TOYOBO, Japan) as described previously [24, 38]. Primers used for Oct3/4, Sox2, Klf4 and c-Myc were designed to detect the expressions of endogenous genes, but not of transgenes. To detect SeV genome, nested RT-PCR was performed. The sequences of primers and amplification conditions are listed in Table S1.

## Cell staining and Immunocytochemistry

Alkaline phosphatase staining was performed using the Leukocyte Alkaline Phosphatase kit (SIGMA). For immunocytochemistry, cells were fixed with PBS containing 4% paraformaldehyde for 30 min at 4℃. For the molecules localized in nucleus, samples were treated with 0.2% Triton X-100 for 15 min at room temperature (RT). The cells were washed three times with PBS containing 2% FBS and then incubated overnight at 4℃ in PBS containing 2% FBS with primary antibodies. The list of the primary and secondary antibodies is described in Table S2.

## Southern blotting

TCR probe was amplified by PCR as described previously using cDNA of human peripheral blood mononuclear cells and labeled with $\alpha^{32}$P-dCTP by BcaBEST labeling Kit (Takara Bio Co. Ltd). Commercially available membranes–Hybond-$N^+$ (GE Healthcare) were used and hybridization was performed as described previously [38].

## Differentiation into three germ layer cells

Mesoderm-like cell cultures were specified based upon a previously described protocol [39]. For the embryoid body (EB) formation, iPSC clusters were

transferred to low attachment dishes in DMEM/F12 (SIGMA) supplemented with 20% KSR (Invitrogen) and 10 ng/ml BMP4 (R & D). Next day, the formed EBs were transferred to collagen IV-coated tissue culture plates (BD) in the medoserm induction medium containing alpha-MEM supplemented with 10% FBS, 0.1 mM 2ME, 3 ng/ml Activin (R & D) 10 ng/ml BMP4 and 5 ng/ml bFGF (WAKO). On day 4, the cells were harvested and analyzed for BRACHYURY expression. For endoderm-like cell induction, the culture medium of semi-confluent human iPS cells were switched from the iPS medium to the definitive endoderm differentiation medium containing RPMI1640 supplemented with 2% B27 (Life technologies), 100 ng/ml Activin A (R & D) and 1 mM Sodium butyrate (NaB, SIGMA). The NaB concentration is changed in 0.5 mM on day 2. On day4, the cells were stained with anti-SOX17 antibody.

For neural cell induction, the iPSC clusters were plated onto Geltrex plates (Life Technologies). 24 hours later, the culture medium was switched from the iPSC medium to PSC Neural Induction Medium (Life Technologies) containing Neurobasal medium and PSC neural induction supplement [40]. On day 7, the cells were dissociated with TrypLE express (Life Technologies) and re-seeded onto Geltrex-coated plates in NSC expansion medium containing 50% Neurobasal medium, 50% Advanced DMEM/F12, neural induction supplement and 5 μM Rock inhibitor, Y-27632. On day 14, the cells were stained with anti-betaIII tubulin antibody.

### Teratoma formation

Human and chimpanzee iPSC lines grown on MEF feeder layers were collected by collagenase IV treatment and injected into the testis of NOD-SCID immunodeficient mice. Palpable tumors were observed about 12–16 weeks after injection. Tumor samples were collected, fixed in 10% formalin, and processed for paraffin-embedding and hematoxylin-eosin staining following standard procedures.

### Microarray analysis

Two hundred fifty ng of total RNA from the chimpanzee iPSCs were labeled with biotin and fragmented according to the manufacturer's protocol (3′ IVT Express kit, Affymetrix). Then, samples were hybridized to a GeneChip Human Genome U133 Plus 2.0 (Affymetrix) Arrays were scanned with a GeneChip Scanner 3000(Affymetrix). Data were analyzed using GeneSpring GX 12.5 software (Agilent technologies). Each chip is normalized to the median of the measurements.

## Supporting Information

**Figure S1.** iPS cell generation with SeV vector carrying *L-Myc* and *Glis1*. (**a**) Schematic structure of Sendai virus (SeV) vectors carrying *L-Myc* and *Glis1*. The exogenous *L-Myc* cDNA is inserted between HN and L positions in TS15 vector.

*Glis1* cDNA were inserted between HN and L positions in conventional and TS15 SeV vectors, HNL/TS Glis1 and HNL/TS15 Glis1. We also generated other two vectors, +18/TS Glis1 and +18/TS15 Glis1, which carry Glis1 in the downstreams of Leader in conventional and TS15 SeV vectors. (**b**) Efficiency of iPS cell generation with Myc vectors. The efficiency of iPS cell generation is much lower by *L-Myc* SeV vector than by *c-Myc* SeV vector. iPS cell colonies were identified on day 28 of induction by the appearance of alkaline phosphatase-positive (AP+) colonies with ES cell-like colony morphology. Colony number (right picture) were counted and summarized in left graph. MOI: multiplicity of infection. (**c**) Efficiency of iPS cell generation with various Glis1 vectors. iPS cells were generated with the three factors (K, O, S) plus *Glis1* in the presence (left graph) and absence (right graph) of *c-Myc*. Both cases showed that *Glis1* in SeV vectors did not enhance the efficiency of iPS cell generation.
doi:10.1371/journal.pone.0113052.s001 (TIF)

**Figure S2.** Experimental design of iPSC induction from chimpanzee blood cells. After collecting mononuclear cells (MNCs) from the chimpanzee blood, MNCs were stimulated with anti-CD3 antibody (Exp. 1) or Con A (Exp. 2 and 3) for five days. One day later after the infection of the sendai virus carrying *OCT3/4*, *KLF4*, *SOX2* and *cMYC*, the cells were transferred on the MEFs with 5 ng/ml (Exp. 1) or 30 ng/ml (Exp.2 and 3) FGF2.
doi:10.1371/journal.pone.0113052.s002 (TIF)

**Figure S3.** Comparing the chimpanzee with human conditions in iPSC generation. Using human blood cells from two volunteers (volunteer 4 and 5), the condition of chimpanzee with 30 ng/ml FGF2 is compared with that of human with 5 ng/ml in iPSC generation. The efficiency of iPSC generation with 30 ng/ml FGF is slightly but not significantly lower than that with 5 ng/ml FGF2.
doi:10.1371/journal.pone.0113052.s003 (TIF)

**Table S1.** Sequences and PCR conditions of primers sets for PCR.
doi:10.1371/journal.pone.0113052.s004 (DOCX)

**Table S2.** List of antibodies and their conditions for staining.
doi:10.1371/journal.pone.0113052.s005 ((DOCX))

## Author Contributions

Conceived and designed the experiments: TE. Performed the experiments: YF TK M. Hamasaki YS MS NF. Analyzed the data: YF TK M. Hamasaki YS MS NF. Contributed reagents/materials/analysis tools: NF HB M. Hasegawa SY SK SS TM HA. Wrote the paper: TE.

## References

1. **Takahashi K, Yamanaka S** (2006) Induction of pluripotent stem cells from mouse embryonic and adult fibroblast cultures by defined factors. Cell 126: 663–676.

2. **Liao J, Cui C, Chen S, Ren J, Chen J, et al.** (2009) Generation of induced pluripotent stem cell lines from adult rat cells. Cell Stem Cell 4: 11–15.

3. **Tomioka I, Maeda T, Shimada H, Kawai K, Okada Y, et al.** (2010) Generating induced pluripotent stem cells from common marmoset (Callithrix jacchus) fetal liver cells using defined factors, including Lin28. Genes Cells 15: 959–969.

4. **Liu H, Zhu F, Yong J, Zhang P, Hou P, et al.** (2008) Generation of induced pluripotent stem cells from adult rhesus monkey fibroblasts. Cell Stem Cell 3: 587–590.

5. **Takahashi K, Tanabe K, Ohnuki M, Narita M, Ichisaka T, et al.** (2007) Induction of pluripotent stem cells from adult human fibroblasts by defined factors. Cell 131: 861–872.

6. **Wu Z, Chen J, Ren J, Bao L, Liao J, et al.** (2009) Generation of pig induced pluripotent stem cells with a drug-inducible system. J Mol Cell Biol 1: 46–54.

7. **Wu Y, Zhang Y, Mishra A, Tardif SD, Hornsby PJ** (2010) Generation of induced pluripotent stem cells from newborn marmoset skin fibroblasts. Stem Cell Res 4: 180–188.

8. **Hankowski KE, Hamazaki T, Umezawa A, Terada N** (2011) Induced pluripotent stem cells as a next-generation biomedical interface. Lab Invest 91: 972–977.

9. **Hackett TA, Preuss TM, Kaas JH** (2001) Architectonic identification of the core region in auditory cortex of macaques, chimpanzees, and humans. J Comp Neurol 441: 197–222.

10. **Rogers J, Gibbs RA** (2014) Comparative primate genomics: emerging patterns of genome content and dynamics. Nat Rev Genet 15: 347–359.

11. **Mubiru JN, Yang AS, Olsen C, Nayak S, Livi CB, et al.** (2014) Analysis of prostate-specific antigen transcripts in chimpanzees, cynomolgus monkeys, baboons, and African green monkeys. PLoS One 9: e94522.

12. **Rearden A** (1986) Evolution of glycophorin A in the hominoid primates studied with monoclonal antibodies, and description of a sialoglycoprotein analogous to human glycophorin B in chimpanzee. J Immunol 136: 2504–2509.

13. **Gonzalez JP, Prugnolle F, Leroy E** (2013) Men, primates, and germs: an ongoing affair. Curr Top Microbiol Immunol 365: 337–353.

14. **Wernig M, Meissner A, Foreman R, Brambrink T, Ku M, et al.** (2007) In vitro reprogramming of fibroblasts into a pluripotent ES-cell-like state. Nature 448: 318–324.

15. **Sommer CA, Stadtfeld M, Murphy GJ, Hochedlinger K, Kotton DN, et al.** (2009) Induced pluripotent stem cell generation using a single lentiviral stem cell cassette. Stem Cells 27: 543–549.

16. **Woltjen K, Michael IP, Mohseni P, Desai R, Mileikovsky M, et al.** (2009) piggyBac transposition reprograms fibroblasts to induced pluripotent stem cells. Nature 458: 766–770.

17. **Zhou H, Wu S, Joo JY, Zhu S, Han DW, et al.** (2009) Generation of induced pluripotent stem cells using recombinant proteins. Cell Stem Cell 4: 381–384.

18. **Miyoshi N, Ishii H, Nagano H, Haraguchi N, Dewi DL, et al.** (2011) Reprogramming of mouse and human cells to pluripotency using mature microRNAs. Cell Stem Cell 8: 633–638.

19. **Okita K, Nakagawa M, Hyenjong H, Ichisaka T, Yamanaka S** (2008) Generation of mouse induced pluripotent stem cells without viral vectors. Science 322: 949–953.

20. **Seki T, Yuasa S, Oda M, Egashira T, Yae K, et al.** (2010) Generation of induced pluripotent stem cells from human terminally differentiated circulating T cells. Cell Stem Cell 7: 11–14.

21. **Okita K, Yamakawa T, Matsumura Y, Sato Y, Amano N, et al.** (2013) An efficient nonviral method to generate integration-free human-induced pluripotent stem cells from cord blood and peripheral blood cells. Stem Cells 31: 458–466.

22. **Fusaki N, Ban H, Nishiyama A, Saeki K, Hasegawa M** (2009) Efficient induction of transgene-free human pluripotent stem cells using a vector based on Sendai virus, an RNA virus that does not integrate into the host genome. Proc Jpn Acad Ser B Phys Biol Sci 85: 348–362.

23. **Ban H, Nishishita N, Fusaki N, Tabata T, Saeki K, et al.** (2011) Efficient generation of transgene-free human induced pluripotent stem cells (iPSCs) by temperature-sensitive Sendai virus vectors. Proc Natl Acad Sci U S A 108: 14234–14239.

24. **Hamasaki M, Hashizume Y, Yamada Y, Katayama T, Hohjoh H, et al.** (2012) Pathogenic mutation of ALK2 inhibits induced pluripotent stem cell reprogramming and maintenance: mechanisms of reprogramming and strategy for drug identification. Stem Cells 30: 2437–2449.

25. **Nakagawa M, Takizawa N, Narita M, Ichisaka T, Yamanaka S** (2010) Promotion of direct reprogramming by transformation-deficient Myc. Proc Natl Acad Sci U S A 107: 14152–14157.

26. **Maekawa M, Yamaguchi K, Nakamura T, Shibukawa R, Kodanaka I, et al.** (2011) Direct reprogramming of somatic cells is promoted by maternal transcription factor Glis1. Nature 474: 225–229.

27. **Mali P, Chou BK, Yen J, Ye Z, Zou J, et al.** (2010) Butyrate greatly enhances derivation of human induced pluripotent stem cells by promoting epigenetic remodeling and the expression of pluripotency-associated genes. Stem Cells 28: 713–720.

28. **McLean CY, Reno PL, Pollen AA, Bassan AI, Capellini TD, et al.** (2011) Human-specific loss of regulatory DNA and the evolution of human-specific traits. Nature 471: 216–219.

29. **Langerak AW, Wolvers-Tettero IL, van Dongen JJ** (1999) Detection of T cell receptor beta (TCRB) gene rearrangement patterns in T cell malignancies by Southern blot analysis. Leukemia 13: 965–974.

30. **Nakagawa M, Koyanagi M, Tanabe K, Takahashi K, Ichisaka T, et al.** (2008) Generation of induced pluripotent stem cells without Myc from mouse and human fibroblasts. Nat Biotechnol 26: 101–106.

31. **Stadtfeld M, Nagaya M, Utikal J, Weir G, Hochedlinger K** (2008) Induced pluripotent stem cells generated without viral integration. Science 322: 945–949.

32. **Soldner F, Hockemeyer D, Beard C, Gao Q, Bell GW, et al.** (2009) Parkinson's disease patient-derived induced pluripotent stem cells free of viral reprogramming factors. Cell 136: 964–977.

33. **Nagai Y TA, Irie T, Yonemitsu Y, Gotoh B** (2011) Sendai virus: Evolution from mouse pathogen to a state-of-the-art tool in virus research and biotechnology. The biology of Paramyxoviruses Samal SK, Ed, Caister Academic Press, Norfolk, UK: 115–173.

34. **Kehrer-Sawatzki H, Cooper DN** (2007) Understanding the recent evolution of the human genome: insights from human-chimpanzee genome comparisons. Hum Mutat 28: 99–130.

35. **Marchetto MC, Narvaiza I, Denli AM, Benner C, Lazzarini TA, et al.** (2013) Differential L1 regulation in pluripotent stem cells of humans and apes. Nature 503: 525–529.

36. **Sasaki K, Inoue M, Shibata H, Ueda Y, Muramatsu SI, et al.** (2005) Efficient and stable Sendai virus-mediated gene transfer into primate embryonic stem cells with pluripotency preserved. Gene Ther 12: 203–210.

37. **Fusaki N BH, Nagai Y** (2014) Induction of Human Pluripotent Stem Cells by the Sendai Virus Vector: Establishment of a Highly Efficient and Footprint-Free System. Sendai Virus Vector: Advantages and Applications Springer 171–183.

38. **Kitagawa M, Takebe A, Ono Y, Imai T, Nakao K, et al.** (2012) Phf14, a novel regulator of mesenchyme growth via platelet-derived growth factor (PDGF) receptor-alpha. J Biol Chem 287: 27983–27996.

39. **Sakurai H, Era T, Jakt LM, Okada M, Nakai S, et al.** (2006) In vitro modeling of paraxial and lateral mesoderm differentiation reveals early reversibility. Stem Cells 24: 575–586.

40. **Yan Y, Shin S, Jha BS, Liu Q, Sheng J, et al.** (2013) Efficient and rapid derivation of primitive neural stem cells and generation of brain subtype neurons from human pluripotent stem cells. Stem Cells Transl Med 2: 862–870.

nature COMMUNICATIONS

ARTICLE

Received 8 Dec 2013 | Accepted 31 Jan 2014 | Published 26 Feb 2014

DOI: 10.1038/ncomms4368

# Regulation of MKL1 via actin cytoskeleton dynamics drives adipocyte differentiation

Hiroyuki Nobusue[1,2], Nobuyuki Onishi[2], Takatsune Shimizu[2,3], Eiji Sugihara[2,3], Yoshinao Oki[1], Yuko Sumikawa[1], Tatsuyuki Chiyoda[2], Koichi Akashi[4], Hideyuki Saya[2,3] & Koichiro Kano[1]

Cellular differentiation is regulated through activation and repression of defined transcription factors. A hallmark of differentiation is a pronounced change in cell shape, which is determined by dynamics of the actin cytoskeleton. Here we show that regulation of the transcriptional coactivator MKL1 (megakaryoblastic leukemia 1) by actin cytoskeleton dynamics drives adipocyte differentiation mediated by peroxisome proliferator-activated receptor γ (PPARγ), a master transcriptional regulator of adipogenesis. Induction of adipocyte differentiation results in disruption of actin stress fibres through downregulation of RhoA-ROCK signalling. The consequent rapid increase in monomeric G-actin leads to the interaction of G-actin with MKL1, which prevents nuclear translocation of MKL1 and allows expression of PPARγ followed by adipogenic differentiation. Moreover, we found that MKL1 and PPARγ act in a mutually antagonistic manner in the adipocytic differentiation programme. Our findings thus provide new mechanistic insight into the relation between the dynamics of cell shape and transcriptional regulation during cellular differentiation.

[1] Laboratory of Cell and Tissue Biology, College of Bioresource Sciences, Nihon University, Fujisawa, Kanagawa 252-0880, Japan. [2] Division of Gene Regulation, Institute for Advanced Medical Research, Keio University School of Medicine, Tokyo 160-8582, Japan. [3] Japan Science and Technology Agency, Core Research for Evolutional Science and Technology (CREST), Tokyo 102-0076, Japan. [4] Department of Medicine and Biosystemic Science, Kyushu University Graduate School of Medical Science, Fukuoka 812-8582, Japan. Correspondence and requests for materials should be addressed to H.S. (email: hsaya@a5.keio.jp) or to K.K. (email: kano.kouichirou@nihon-u.ac.jp).

Activation and repression of defined transcription factors are essential for the commitment of progenitors to a specific differentiation lineage, setting the stage for a gene expression pattern characteristic of each mature cell type[1–3]. Adipocyte differentiation is regulated by multiple transcription factors, with PPARγ and members of the CCAAT/enhancer-binding protein (C/EBP) family having central roles. Cooperative interactions among these transcription factors drive the expression of downstream target genes that are necessary for the generation and maintenance of adipocyte characteristics such as lipid accumulation and insulin sensitivity[4]. The key role of PPARγ in the commitment of mesenchymal precursors to the adipocytic differentiation programme is evident from the observation that forced expression of this protein stimulates adipogenesis in nonadipogenic fibroblastic cell lines, such as NIH 3T3 and 3T3-C2 (refs 5,6). PPARγ is thus thought to function as an adipocyte-specific master switch in acquisition of the adipocytic phenotype[7].

The adipocytic differentiation of fibroblastic preadipocytes is accompanied by the adoption of a rounded morphology that is characteristic of mature adipocytes and allows for maximal lipid storage[8]. Cell morphology is determined primarily by the actin cytoskeleton[9]. Adipocyte differentiation is thus associated with a shift in the structures formed by filamentous (F) actin from stress fibres to cortical fibres[10,11]. The relation between such reorganization of the actin cytoskeleton and the PPARγ-mediated adipocytic differentiation programme has remained unclear, however.

We have previously established a preadipocyte cell line derived from mouse dedifferentiated fat (DFAT) cells and which possesses a higher potential to differentiate into adipocytes compared with the mouse preadipocyte cell line 3T3-L1 (ref. 12). Unlike 3T3-L1 cells, these DFAT cells do not undergo spontaneous adipogenesis, with the adipocytic differentiation of DFAT cells thus being more tightly controlled than that of 3T3-L1 cells[12,13]. Here, we examine the roles of actin cytoskeleton remodelling in adipocytic differentiation by using DFAT cells. We show that the rapid disruption of actin stress fibres through downregulation of RhoA-ROCK signalling and the consequent increase in monomeric G-actin levels are observed before adipocyte differentiation. We also found that interaction of monomeric G-actin with the transcriptional coactivator MKL1 is the key event for initiating PPARγ expression. Moreover, MKL1 and PPARγ were shown to act in a mutually antagonistic manner in the adipocytic differentiation programme. Our findings provide a new insight into the regulatory mechanism of adipocyte differentiation.

## Results

**Adipogenesis requires disruption of actin stress fibres.** We first examined the changes in the actin cytoskeleton and PPARγ expression during adipogenesis with the use of an established DFAT cell line. Before induction of adipogenesis, DFAT cells manifest a fibroblastic morphology with well-developed actin stress fibres (Fig. 1a). At 24 h after the induction of adipocytic differentiation with the combination of 3-isobutyl-1-methylxanthine (IBMX), dexamethasone and insulin, the cells exhibit a well-spread morphology associated with the disruption of most stress fibres (Fig. 1a,c; Supplementary Movie 1). The upregulation of PPARγ expression at both mRNA and protein levels is evident at 48 h (Fig. 1a,b), at which time the cell morphology has become stellate and the cortical actin structures characteristic of adipocytes are evident (Fig. 1a). The expression of perilipin (a marker of terminal adipocyte differentiation) and the accumulation of lipid droplets are observed from 60 h, at which time the cell morphology has become more rounded (Fig. 1a). Together, these results thus suggested that disruption of actin stress fibres precedes the induction of PPARγ expression during adipocyte differentiation.

Previous studies have shown that actin cytoskeleton dynamics associated with cell rounding in response to mechanical or physical stimuli (such as matrix stiffness and cytoskeletal tension) result in adipogenic differentiation of 3T3-F442A preadipocytes or mesenchymal stem cells by a mechanism that involves RhoA-ROCK (Rho-kinase) signalling[14–18], which regulates the formation of actin stress fibres and focal adhesions[19,20]. On the other hand, ectopic expression of PPARγ in mesenchymal stem cells or NIH 3T3 fibroblasts has been found to induce not only expression of adipose-specific genes but also morphological differentiation, including the accumulation of triglyceride droplets[5,21–24]. It has remained unknown, however, whether the pathways underlying the induction of adipogenesis either by PPARγ or by changes in cell shape operate independently of each other or in an interdependent manner. To address this question, we tested the effects both of RNA interference (RNAi)-mediated depletion of cofilin1, a protein that promotes the disassembly of actin filaments[25], and of phalloidin (a cytoskeletal fixative) on PPARγ expression during adipocyte differentiation. Either knockdown of cofilin1 with specific small interfering RNAs (siRNAs) or treatment with phalloidin blocked the disruption of actin stress fibres as well as markedly inhibited both the upregulation of PPARγ and PPARγ target gene expression and the accumulation of lipid droplets elicited by inducers of adipocyte differentiation in DFAT cells and 3T3-L1 preadipocytes (Fig. 1d,e; Supplementary Fig. 1). These data thus indicated that the disruption of actin stress fibres is required

**Figure 1 | Disruption of actin stress fibres is required for adipocyte differentiation.** (**a**) Fluorescence microscopy of the actin cytoskeleton (stained with phalloidin) as well as of PPARγ or perilipin expression during adipogenesis in DFAT cells. Nuclei were stained with Hoechst 33342 (blue fluorescence). Scale bars, 20 μm. (**b**) Relative abundance of *Pparg* mRNA during adipocytic differentiation in DFAT cells (left panel). (**a–f**) $P<0.05$, Tukey's honest significant difference test. A nuclear fraction prepared from the cells was also subjected to immunoblot analysis of PPARγ and lamin C (loading control) (right panel). (**c**) Time-lapse imaging of DFAT cells expressing red fluorescent protein (RFP)-tagged actin at the indicated times (hours:minutes). Scale bars, 50 μm. (**d**) 3T3-L1 preadipocytes transfected with cofilin1 (si*Cfl1*-a) or control (si*Control*) siRNAs were exposed to inducers of differentiation for 96 h. They were then subjected to fluorescence microscopic analysis of the actin cytoskeleton and PPARγ expression. Nuclei were stained with Hoechst 33342. Scale bars, 50 μm. Relative abundance of *Pparg*, *Cebpa*, *Fabp4*, *Slc2a4* and *Plin1* mRNAs. *$P<0.05$, Student's *t*-test. (**e**) Oil red O (ORO) staining of cells treated as in **d**. Bars, 100 μm. The absorbance at 510 nm ($A_{510}$) of dye extracted from the stained cells was also determined. *$P<0.05$, Student's *t*-test. (**f**) Immunoblot analysis of active and total forms of Rho proteins during adipocyte differentiation in DFAT cells (left panels). GAPDH was examined as a loading control. Quantification of the immunoblotting data was performed using densitometry. Data were normalized to the amount of total Rho (right panel). *$P<0.05$, Student's *t*-test. n.s., not significant. (**g**) Fluorescence microscopy of the actin cytoskeleton as well as of PPARγ or perilipin expression in DFAT cells expressing HA-tagged RhoAV14 or RhoAN19 and exposed for 96 h to inducers of differentiation in the absence or presence of Y-27632 (30 μM) or CytD (0.2 μM). Nuclei were stained with Hoechst 33342. Scale bars, 20 μm. At least 50 HA-positive cells were scored for determination of the percentage of those expressing PPARγ. *$P<0.05$, Student's *t*-test. All quantitative data are means ± s.d. ($n=3$ experiments fibres).

for the induction of PPARγ expression during adipocyte differentiation.

**RhoA-ROCK signalling regulates adipogenesis.** We next investigated whether RhoA-ROCK signalling plays a role in adipogenic differentiation dependent on the disruption of actin stress fibres in DFAT cells. The GTP-bound (active) form of Rho proteins was detected at a high level before adipogenic induction and was markedly reduced in abundance within 24 h after exposure of the cells to inducers of adipocyte differentiation

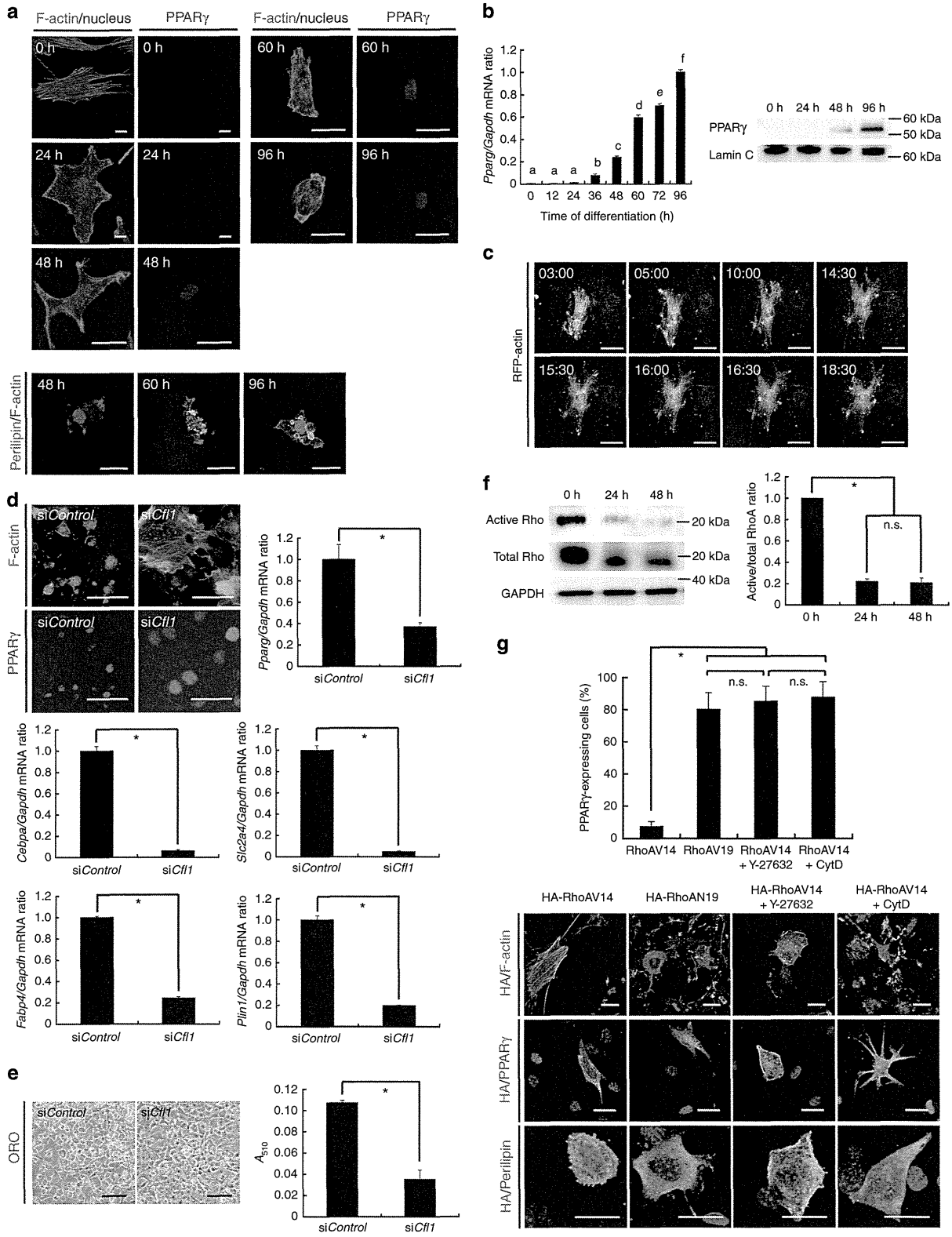

(Fig. 1f). We transiently transfected DFAT cells with plasmids encoding hemagglutinin epitope (HA)–tagged dominant active (RhoAV14) or dominant negative (RhoAN19) mutants of RhoA and then exposed the cells to inducers of adipocytic differentiation for 96 h. Expression of RhoAV14 inhibited both remodelling of the actin cytoskeleton as well as the induction of PPARγ and perilipin expression, and these inhibitory effects were prevented by treatment with the ROCK inhibitor Y-27632 (Fig. 1g). We also determined whether the effects of ROCK inhibition in RhoAV14-expressing cells were mimicked by the actin-depolymerizing agent cytochalasin D (CytD). The addition of CytD indeed restored remodelling of the actin cytoskeleton as well as the expression of PPARγ and perilipin in RhoAV14-expressing cells to levels similar to those apparent in RhoAV14-expressing cells treated with Y-27632 or in cells expressing RhoAN19 (Fig. 1g). These results thus indicated that RhoA-ROCK signalling regulates adipocyte differentiation through control of remodelling of the actin cytoskeleton.

**G-actin induces adipogenesis by controling MKL1 localization.** Recent studies have identified mechanisms by which actin dynamics directly affect gene transcription[26]. Monomeric G-actin binds to the transcriptional coactivator MKL1 (also known as MAL or MRTF-A) and prevents it from translocating to the nucleus and activating transcription[27,28]. Furthermore, in multipotent mesenchymal stem cells, Med23 functions as a molecular switch between ELK1 and MKL1 that controls differentiation into adipocytes or smooth muscle cells[29], suggesting links between MKL1 and adipogenesis. To explore whether the control of MKL1 translocation by cellular G-actin contributes to the regulation of PPARγ expression and adipocyte differentiation, we established DFAT cells expressing mCherry fused to MKL1 (mCherry-MKL1; Supplementary Fig. 2a) and investigated G-actin levels and mCherry-MKL1 localization before and after the induction of adipocyte differentiation. F-actin was rapidly depolymerized to monomeric G-actin after the induction of adipocyte differentiation, with the increase in cellular G-actin concentration (Fig. 2a). mCherry-MKL1 was detected exclusively in the nucleus before adipogenic induction but was predominantly pancellular and/or cytoplasmic after the induction of adipogenesis (Fig. 2a). PPARγ expression was detected in cells having the cytoplasmic localization of mCherry-MKL1 (Supplementary Fig. 2b).

We next tested whether actin-depolymerizing agents latrunculin A (LatA), which increases monomeric G-actin[27,30], or swinholide A (SwinA), which increases dimeric actin that does not interact with MKL1 (refs 27,30,31), might mimic the effects of inducers of adipogenesis on dynamics of the actin cytoskeleton and MKL1 localization in DFAT cells expressing mCherry-MKL1. Indeed, LatA or SwinA induced disruption of actin stress fibres and increased the cellular abundance of G-actin monomers or dimers, respectively (Fig. 2b; Supplementary Fig. 2c). LatA treatment caused the cytoplasmic sequestration of mCherry-MKL1, whereas SwinA treatment resulted in the nuclear localization (Fig. 2b). Furthermore, LatA alone induced a significant increase in the expression of PPARγ and PPARγ target genes unlike SwinA (Fig. 2c,d). These results suggested that monomeric G-actin formation leads to adipocyte differentiation by blocking the nuclear import of MKL1, but not by other consequences of disruption of actin stress fibres. Similarly to LatA, treatment with Y-27632, elicited disruption of actin stress fibres and the cytoplasmic sequestration of MKL1, resulting in a marked increase in the expression of PPARγ and PPARγ-target genes as well as in the accumulation of lipid droplets in DFAT cells and 3T3-L1 preadipocytes (Supplementary Fig. 3).

**Adipogenesis requires interaction between G-actin and MKL1.** We also asked whether the interaction between G-actin and MKL1 and the consequent cytoplasmic sequestration of MKL1 contribute to adipocyte differentiation. To address this issue, we established DFAT cells and 3T3-L1 preadipocytes that express a FLAG epitope–tagged fusion protein of the oestrogen receptor (ER) and either MKL1 or a deletion mutant of MKL1 (MKL1-N100) that lacks the 100 $NH_2$-terminal amino acids of the full-length protein and therefore does not contain the RPEL actin-binding domain[32,33] (Supplementary Fig. 4a). Exposure of these cells to the ER agonist 4-hydroxytamoxifen (TAM) induced the nuclear translocation of each fusion protein (Fig. 3a). The nuclear translocation of ER-MKL1 was accompanied by a marked decrease in the expression of PPARγ and PPARγ target genes as well as in the accumulation of lipid droplets in cells also exposed to inducers of adipocytic differentiation (Fig. 3b–d; Supplementary Fig. 4b–d). Moreover, expression of ER-MKL1-N100, which fails to bind G-actin and a substantial proportion of which was localized to the nucleus even in the absence of TAM (Fig. 3b; Supplementary Fig. 4b), resulted in marked suppression of adipogenesis in the absence or presence of TAM compared with that apparent in cells expressing ER-MKL1 (Fig. 3b–d; Supplementary Fig. 4b–d). We also tested if ER-MKL1-N100 reverts the effects elicited by treatment with LatA in DFAT cells and 3T3-L1 preadipocytes. The expression of ER-MKL1-N100, which was predominantly localized to the nucleus even after treatment with LatA and remarkably impaired the expression of PPARγ and PPARγ target genes compared with that of ER-MKL1 (Fig. 3e,f; Supplementary Fig. 4e,f). These findings significantly strengthen our conclusion that the increase in the cytoplasmic abundance of G-actin triggers adipocyte differentiation via regulation of the subcellular localization of MKL1.

**Loss of MKL1 drives adipocyte differentiation.** We further assessed whether RNAi-mediated depletion of MKL1 alone might induce PPARγ expression and adipocyte differentiation in the absence of an adipogenic cocktail. In both DFAT cells and 3T3-L1

**Figure 2 | The increase of G-actin accumulation resulting from disruption of actin stress fibres is involved in the cytoplasmic sequestration of MKL1 and adipocyte differentiation in DFAT cells.** (**a**) Immunofluorescence analysis of mCherry and G-actin (stained with DNase I) in cells stably expressing mCherry-MKL1 at 0 or 48 h after the induction of adipogenesis(upper panels). Nuclei were stained with Hoechst 33342. Scale bars, 100 μm. At least 300 cells per coverslip were scored for determination of the percentage of the subcellular localization of MKL1 (lower panel). N, nuclear; N/C, comparable intensity in nucleus and cytoplasm; C, cytoplasmic. (**b**) Immunofluorescence analysis of mCherry and G-actin in mCherry-MKL1-expressing cells exposed to Lat A (0.4 μM), Swin A (0.1 μM) or dimethyl sulfoxide (DMSO, control) for 6 h in growth medium without an adipogenic cocktail (upper panels). Nuclei were stained with Hoechst 33342. Scale bars, 50 μm. Quantitation of immunofluorescence microscopy; localization of the indicated mCherry-MKL1 was scored in 300 cells as in panel **a** (lower panel). (**c**) Relative abundance of *Pparg*, *Cebpa*, *Fabp4*, *Slc2a4*, and *Plin1* mRNAs in cells treated as in **b**. ND, not detected. (**d**) Cells treated as in **b** were cultured for an additional 18 h (total of 24 h) and then subjected to immunofluorescence analysis of mCherry and PPARγ expression. Nuclei were stained with Hoechst 33342. Scale bars, 50 μm. All quantitative data are means ± s.d. ($n=3$ experiments). *$P<0.05$, Student's *t*-test.